Sensors and Actuators B 254 (2018) 264–271

Contents lists available at ScienceDirect

Sensors and Actuators B: Chemical

journal homepage: www.elsevier.com/locate/snb

Research paper

Tailored periodic Si nanopillar based architectures as highly sensitive universal SERS biosensing platform

Prajith Karadan[a,c], Shantanu Aggarwal[b], Aji A. Anappara[c], Chandrabhas Narayana[b,*], Harish C. Barshilia[a,*]

[a] Nanomaterials Research Laboratory, Surface Engineering Division, CSIR-National Aerospace Laboratories, Bangalore 560017, India
[b] Light Scattering Laboratory, Chemistry and Physics of Materials Unit, Jawaharlal Nehru Centre for Advanced Scientific Research, Bangalore 560064, India
[c] Department of Physics, National Institute of Technology, Calicut 673601, India

ARTICLE INFO

Article history:
Received 15 February 2017
Received in revised form 1 June 2017
Accepted 13 July 2017
Available online 14 July 2017

Keywords:
Si nanpillars
Surface enhanced Raman spectroscopy
Plasmonics
Biomolecule sensing
FDTD

ABSTRACT

We report a skeleton key platform for surface enhanced Raman spectroscopy (SERS) based biosensor, utilizing ordered arrays of Si nanopillars (SiNPLs) with plasmonic silver nanoparticles (AgNPs). The optimized SiNPLs based SERS (SiNPLs-SERS) sensor exhibited high enhancement factor (EF) of 2.4×10^8 for thiophenol with sensitivity down to 10^{-13} M of R6G molecules. The ordered array of SiNPLs stabilizes the distribution of AgNPs along with the light trapping properties, which resulted in high EF and excellent reproducibility. The uniformity in the arrangement of AgNPs makes a single SiNPLs-SERS substrate to work for all types of biomolecules such as positively and negatively charged proteins, hydrophobic proteins, cells and dyes, etc. The experiments conducted on differently charged proteins, amyloid beta (the protein responsible for alzheimers), *E. coli* cells, healthy and malaria infected RBCs provide a proof of concept for employing universal SiNPLs-SERS substrate for trace biomolecule detection. The FDTD simulations substantiate the superior performance of the sensor achieved by the tremendous increase in the hotspot distribution compared to the bare Si sensor.

1. Introduction

Surface enhanced Raman spectroscopy (SERS) is a widely used vibrational spectroscopic technique for potential applications in various fields such as environmental monitoring, chemical and biosensing, biomedical detection, etc. [1–6]. In the recent years, extensive research interest has been focused towards the chemical and biosensing by exploiting the localized surface plasmon resonance (LSPR) on the surface of noble metal nanoparticles [7–10]. The photo-induced electromagnetic field enhancement in the vicinity of metal nanoparticle due to LSPR leads to ultrasensitive probing by SERS [11–13]. An ideal SERS substrate should have (i) high enhancement factor (ii) uniformity in nanoparticle distribution (iii) reproducibility and reusability [14]. The sensitivity of the SERS substrate mainly depends on the enhancement factor, which can be achieved by controlling the size (40–70 nm), interparticle distance (less than 10 nm) and choosing a laser frequency close to the LSPR of the substrate [15–18]. The uniformity of the substrate demands orderly arranged plasmonic nanoparticles on the substrate. The lack of uniformity leads to non-reproducible enhancement and the maximum deviation in the enhancement factor is preferably less than 20% for a good SERS substrate [14].

The plasmonic behavior of noble metal nanoparticles with various sizes and shapes has been widely utilized in two forms: (i) individual and randomly oriented colloidal nanoparticle aggregates (ii) ordered nanostructure arrays [19–21]. The colloidal nanoparticles are generally dispersed in water and possess charged capping agents around them. This makes the detection of oppositely charged and hydrophobic proteins very difficult through SERS. In addition, the difficulty in controlling the localized hot spots and irreproducibility of colloidal nanoparticles have led the researchers to move ahead with the fabrication of heterogeneous solid sensors [22,23]. In the solid sensors, the nanoparticles are arranged or decorated on a micro/nano engineered surface to achieve large area uniform hot spot distributions. There are various techniques for the fabrication of heterogeneous SERS sensors such as reactive ion etching, focused ion beam lithography, E beam lithography, wet etching, etc. [24–27]. Among these methods wet etching is a simple, cost effective fabrication process for achieving uniform nanostructures in large area. Gupta et al. have reported silicon micro-pyramid based SERS sensor, fabricated by wet chemical route with enhance-

* Corresponding authors.
E-mail addresses: cbhas@jncasr.ac.in (C. Narayana), harish@nal.res.in (H.C. Barshilia).

http://dx.doi.org/10.1016/j.snb.2017.07.088
0925-4005/

ment factor 10^6-10^7 for multianalyte detection [28]. However, they have used Si micropyramids as a platform for growing AgNPs, which reduce surface area and number of hot spots in comparison to nanopyramids. Moreover, the non-uniform sized aperiodic micropyramids bring down the reproducibility of the substrate.

Recently, Si nanowires/pillars decorated with metal nanoparticles as SERS sensors are drawing great deal of interest because of their huge surface to volume ratio, unique light trapping properties and high compatibility with the existing silicon technology [29–31]. In the literature, Caldwell et al. have presented Au capped Si nanopillar SERS substrates fabricated using e-beam lithography and RIE etching [32]. The number of hotspots in this case will be less, since the Au is deposited only on the top of the nanopillars (not on the sidewalls). There is a substantial light penetration inside the nanopillars which goes untapped when no nanoparticles are there on the sides. This substrate has shown SERS enhancements for 633 and 785 nm lasers, but did not give any enhancement for 532 nm laser. Gartia et al. have conducted SERS experiments made up of silver coated silica nanopillars [33]. They have fabricated the SERS substrates using high cost laser interference lithography and E-beam evaporation. Moreover, the enhancement was shown only on benzothiophenol analytes and 785 nm laser. In addition, the reported enhancement factor varies from 10^6 to 10^8. The universality and the simplicity of our approach and large enhancement in wide range is because of our preparation of our substrates. Schmidt et al. have reported the metal deposited leaning Si nanopillars as SERS substrates [34]. They have fabricated using e-beam evaporation and reactive ion etching. Their SERS studies are limited for 785 nm wavelength laser and thiophenol. All of them have used high cost instrumentation for the fabrication of SERS substrates. None of them have reported a detailed study on the biosensing using these SERS substrates. Moreover, in literature, most of them have used randomly oriented Si nanowires/pillars for fabricating SERS sensors, which results in irreproducible SERS sensing due to the difficulty in controlling the nanogaps (less than 10 nm) between the nanoparticles. Intuitively, three dimensional nanostructures, which contain highly ordered periodic Si nanowire/pillar arrays with plasmonic nanoparticles can improve the enhancement factor and reproducibility to a great extent. The efficient utilization of these sensors in biomolecule detection can fulfill the widespread applications in the biomedical field. SERS based bio analysis is a label free technique used to identify and characterize microorganisms, living cells, proteins and tissues [35–37]. Siddantha et al. have reported the SERS from oppositely charged proteins using GaN based hybrid SERS substrate for biosensing. This substrate showed relatively low enhancement factor of $\sim 10^5$ and other biomolecules such as cells, microorganism, etc. have not been studied using this substrate [38]. Very recently, Chen et al. have studied the malaria infected RBC using SERS using Ag nanorod substrates [39] Another example for SERS based biosensor is the detection of water-borne pathogens through *E. coli* cells by Zhou et al. [36]. The morphology and nature of the SERS substrate plays a vital role in determining the vibrational modes for biomolecules. Therefore, a single (universal) SERS substrate with high enhancement factor and reproducibility, which works for all types of biomolecules become indispensable.

Herein, we present a simple strategy to fabricate an ultrasensitive, highly reproducible and versatile SERS biosensor based on periodic array of Si nanopillars decorated with AgNPs (SiNPLs-SERS) in a controlled manner. The periodic array of SiNPLs stabilizes the distribution of AgNPs along with the light trapping properties, which result in high enhancement factor ($\sim 10^8$) and excellent reproducibility with a lower detection limit of 10^{-13} M of R6G molecules. The universality of this substrate was verified by the experiments conducted on both positively and negatively charged proteins, hydrophobic proteins (amyloid beta, which is responsible for alzehemiers), normal RBCs and malaria infected RBCs, *E. coli* cells and fluorescent dyes. Further, the near field intensity in the vicinity of AgNPs on the SiNPLs is demonstrated and compared with the bare Si sensor using finite difference time domain (FDTD) simulations.

2. Experimental details

The SiNPL arrays were fabricated using nanosphere lithography and metal assisted chemical etching. Spin coating was used to get a monolayer of polystyrene nanosphere (PS) on the Si wafers. The PS nanospeheres were self assembled in hexagonally close packed arrangement by spin coating and O_2 plasma etching has been performed to separate the PS nanospheres. Gold film of thickness 8–10 nm was coated on the top of PS nanospheres using sputtering. The PS nanospheres were removed after gold coating by sonication using CH_2Cl_2. This results in the formation of nanoporous gold template on the Si wafer. The Si wafers with nanoporous gold template were placed in an etching solution containing HF (40%)/H_2O_2 (30%) and ethanol in the volume ratio 3:1:1, respectively to achieve periodic array of SiNPLs. The SiNPL arrays were deposited with varying thickness of Ag films using magnetron sputtering system. As deposited samples were vacuum annealed at 400 °C for 5 h to achieve the silver nanoparticles of different average diameters. The detailed information about the fabrication of SiNPLs can be found elsewhere [40].

The morphology studied by field emission scanning electron microscopy (FESEM, Carl Zeiss). The absorptance spectra and plasmon modes are observed by UV–vis-NIR spectroscopy (PerkinElmer, Lambda 950). Raman spectrometer with excitation source 532 nm from a diode pumped frequency doubled Nd: YAG solid state laser (PhotopSuwtech Inc., GDLM-5015L) and DILOR-JOBIN-YVON-SPEX with excitation source 633 nm (Model Labram) for He-Ne 20 mW laser beam was used for SERS characterization. LabRam HR Evolution 800, equipped with Horiba iHR 800 monochromator and a Peltier-cooled CCD was used for 785 nm wavelength SERS experiments. The 785 nm, NIR solid state laser made by Horiba was used. For obtaining SERS spectra, 10 μL of the analyte solution of thiophenol and other analytes was dropped on the sensor and allowed to dry. SERS spectra were then collected from three different locations and averaged.

3. Results and discussion

It has been already demonstrated in our previous publications that the vertically aligned SiNPLs with controlled diameter, period and uniformity can be formed using nanosphere lithography and metal assisted chemical etching [40]. The fabricated SiNPLs have size of 70 nm and periodicity of 100 nm. In order to exploit the additional surface area and the three dimensional space provided by the SiNPLs for SERS applications, AgNPs of different average sizes are decorated on the SiNPLs. Fig. 1(a) and (b) shows the FESEM cross-sectional and the top view images of the SiNPLs-SERS sensor with 45 s silver deposition with DC power supply of 5 W. The optimization details of the SiNPLs-SERS sensors are given in Supplementary information Fig. S1. The size distribution of the AgNPs is shown in Fig. 1(c). The corresponding UV–vis spectrum, provided in inset of Fig. 1(c), represents a dipole plasmon mode at 402 nm. The SERS substrates should be excited at its LSPR peak to ensure the effective surface enhanced Raman scattering. Since the UV–vis absorption peak is observed at 400–500 nm, Raman spectrometer with laser source of excitation wavelength $\lambda = 532$ nm has been chosen for the experiments. The enhancement factor (EF) of the optimized SiNPLs-SERS sensor calculated using thiophenol (PhSH) as a model analyte is shown in Fig. 1(d). The highest EF of 2.4×10^8

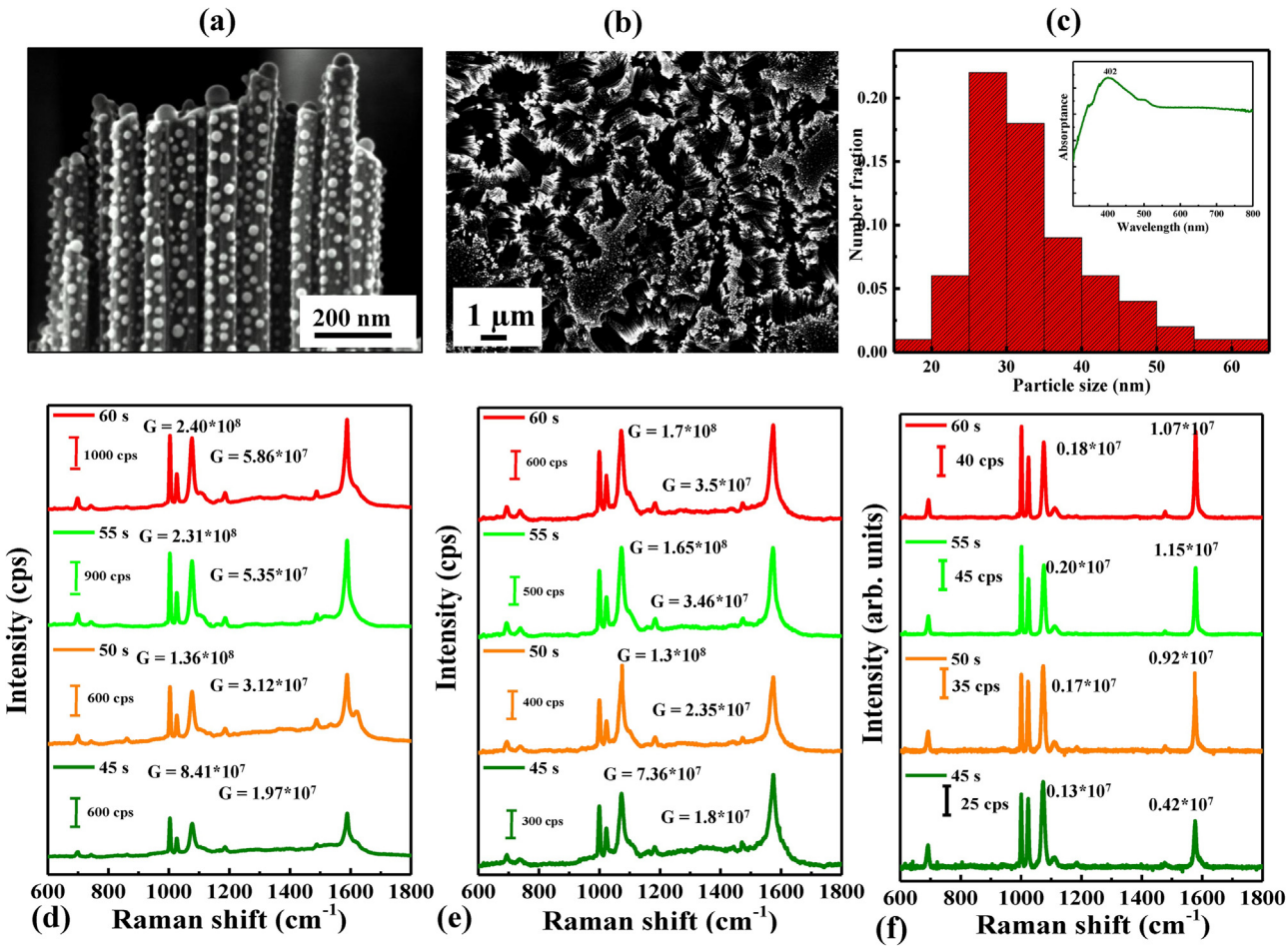

Fig. 1. (a) and (b) FESEM cross-sectional and top view of SiNPLs-SERS sensor (c) Histogram for the AgNP distribution on the SiNPLs for Ag deposition time of 45 s. The corresponding UV–vis spectrum of the SiNPLs-SERS sensor is shown in the inset. (d)–(f) The enhancement factor for the optimized sample with varying Ag deposition time from 45 s–60 s using 532, 633 and 785 nm lasers, respectively.

is observed for SiNPLs-SERS substrates with average roughness of SiNPLs ~629 nm for a silver deposition of 60 s and DC power supply of 5 W. The detailed investigation on the effect of process parameters such as deposition time, surface roughness, etc. on the EF, are presented in Supplementary Fig. S2(a) and (b). The variation of EF with surface roughness of SiNPLs and deposition time of silver are shown in Fig. S3(a).

Most of the SERS substrates are not suitable for sensing with multi-wavelength excitation sources. The laser independence property of the SiNPLs-SERS sensor has been verified by recording the SERS spectra of 1 mM PhSH using laser with excitation wavelengths 633 nm and 785 nm. The SERS spectra of PhSH using 633 and 785 nm lasers are shown in Fig. 1(e) and (f), respectively. All the characteristics peaks of PhSH such as 1001, 1027, 1077 and 1576 cm^{-1} are enhanced significantly without much changes in the EF as compared with the green laser. Based on these observations it is clear that our SiNPLs-SERS sensor can be used for different excitation wavelengths, which economizes biological/chemical material, measurement time, etc. The SERS enhancement of SiNPLs-SERS substrate with 60 s silver deposition using all the three lasers is shown in Supplementary Fig. S3(b) for comparison.

The SERS sensitivity of the SiNPLs-SERS sensor is further investigated with different concentrations of the R6G solution of 10^{-7} M–10^{-13} M and the spectra are shown in Fig. 2(a). A 10^{-3} M solution of R6G was made in water. A series of dilutions were done to make 10^{-6}, 10^{-7}, 10^{-8}, etc. till 10^{-13} M. A 10 µL drop of each of these solutions was drop casted on SiNPL-SERS sensor and it was allowed to get adsorbed and dried. An exponential relationship is obtained for intensity calibration graph between Raman intensity and concentrations of R6G, which is presented in Fig. 2(b). The SERS signal is observable down to 10^{-13} M for R6G and 10^{-12} M for thiophenol, shown in Fig. 2(c), which indicates the very high sensitivity of our SiNPLs-SERS sensor. The ultra sensitivity of SiNPLs-SERS sensor is strongly believed to be due to electromagnetic coupling effect of SiNPLs and AgNPs. The fundamental light coupling property of the SiNPLs has been discussed in our recent publication [41].

The chemical stability of bare nanoparticles on the surface of SiNPLs-SERS sensor makes it a versatile biosensor. Due to the large molecular surface area, SiNPLs are capable of accommodating large biomolecules, which in turn enables better enhancement. This makes SiNPLs useful in biomolecular and disease detection. The uncharged silver nanoparticles of the SiNPLs-SERS sensor were able to produce SERS of both negatively (bovine serum albumin, BSA and human serum albumin, HSA pI = 4.9) charged as well as positively (lysozyme pI = 11.35) charged proteins, presented in Fig. 3(a–c). BSA and HSA are structurally similar to each other and yet they can be differentiated through their SERS spectra. Amyloid beta, a protein responsible for alzheimers disease, is hydrophobic in nature and has an overall negative surface charge. To get the spectrum of hydrophobic amyloid beta, the protein is dissolved in DMSO and further diluted in PBS buffer. A drop of 10^{-6} M of A- beta solution was allowed to dry on the SiNPLs-SERS sensor and the spectrum was recorded with typical acquisition time of 120 s (Fig. 3(d)). Generally, in nanofluidic devices, silica coated nanoparticles or

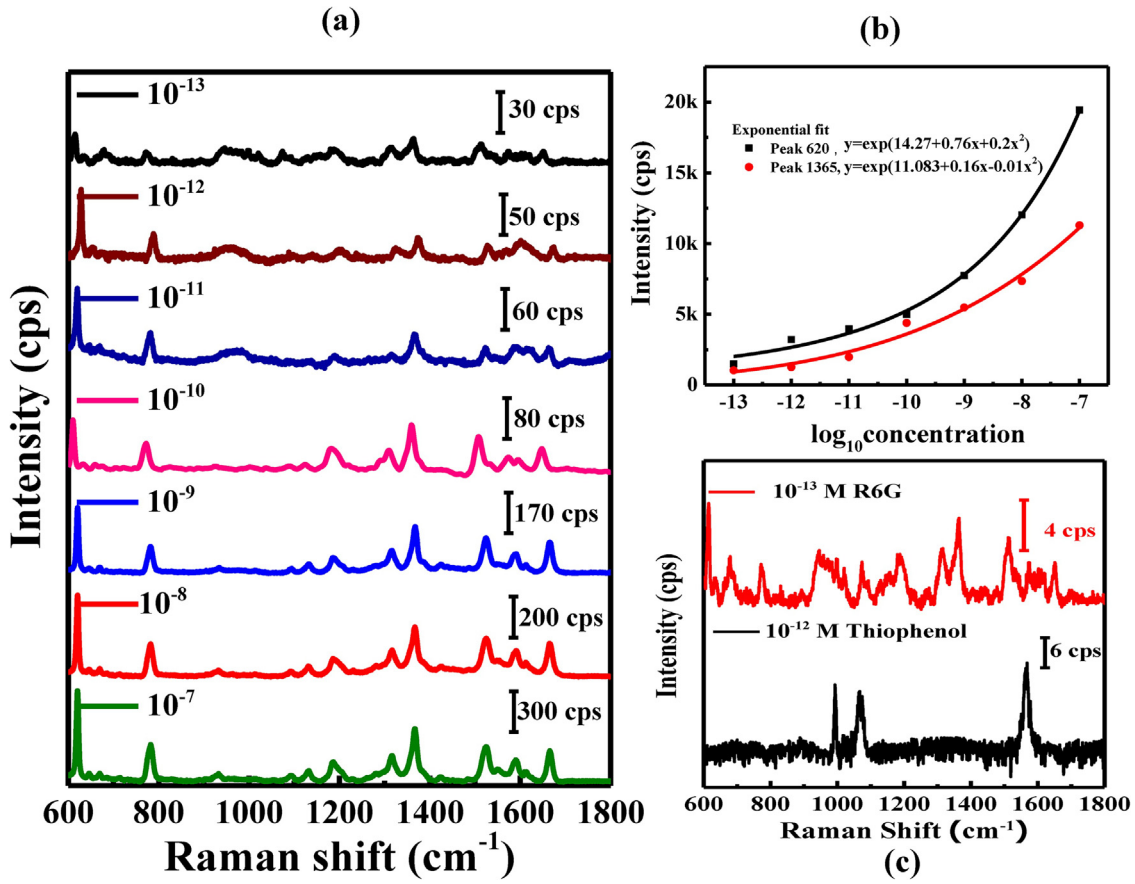

Fig. 2. (a) The SERS spectra of R6G with varying concentration from 10^{-7} to -10^{-13} M. (b) The intensity versus concentration calibration plot for R6G. (c) The SERS spectra of R6G with concentration 10^{-13} M (Red) and thiophenol of 10^{-12} M. (For interpretation of the references to color in this figure legend, the reader is referred to the web version of this article.)

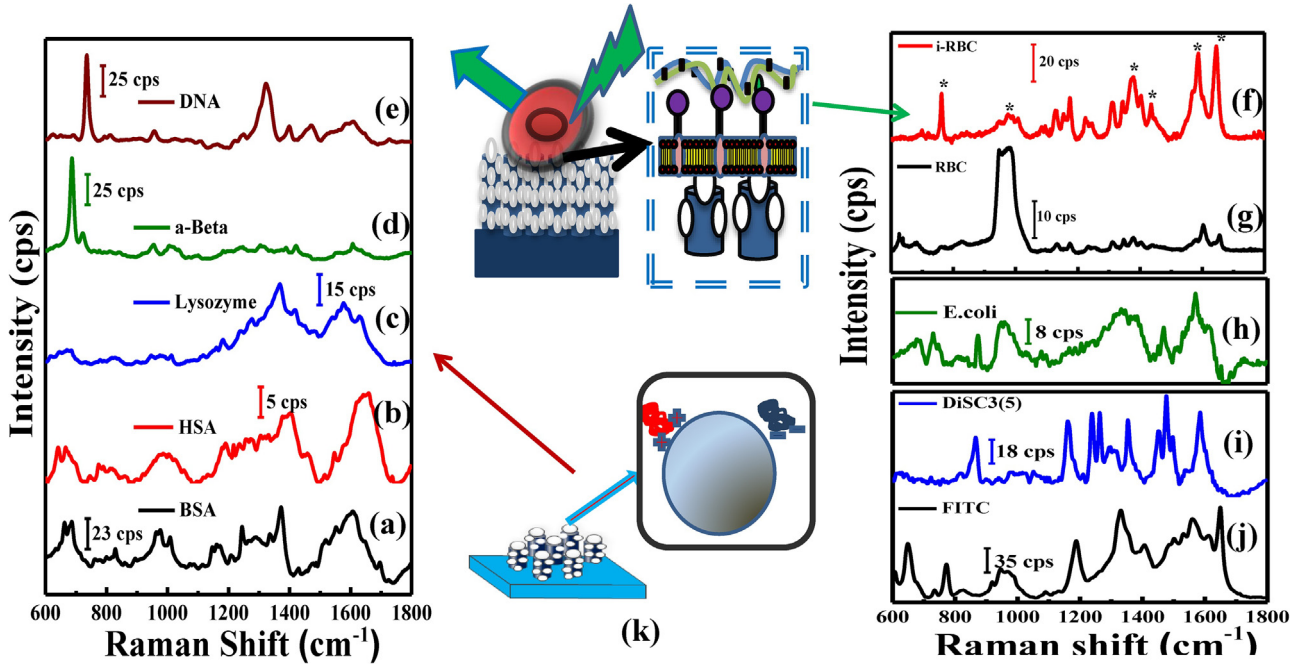

Fig. 3. SERS spectra of (a) and (b) positively charged proteins HSA and BSA (c) negatively charged protein lyzozyme (d) Hydrophobic A- Beta protein (e) DNA (f) and (g) healthy and malaria infected RBC (i-RBC), respectively (h) *E. coli* cells (i) and (j) Disc 3 and FITC dyes. (k) Schematic diagram for the interaction of cells and differently charged proteins with the SiNPLs-SERS sensor.

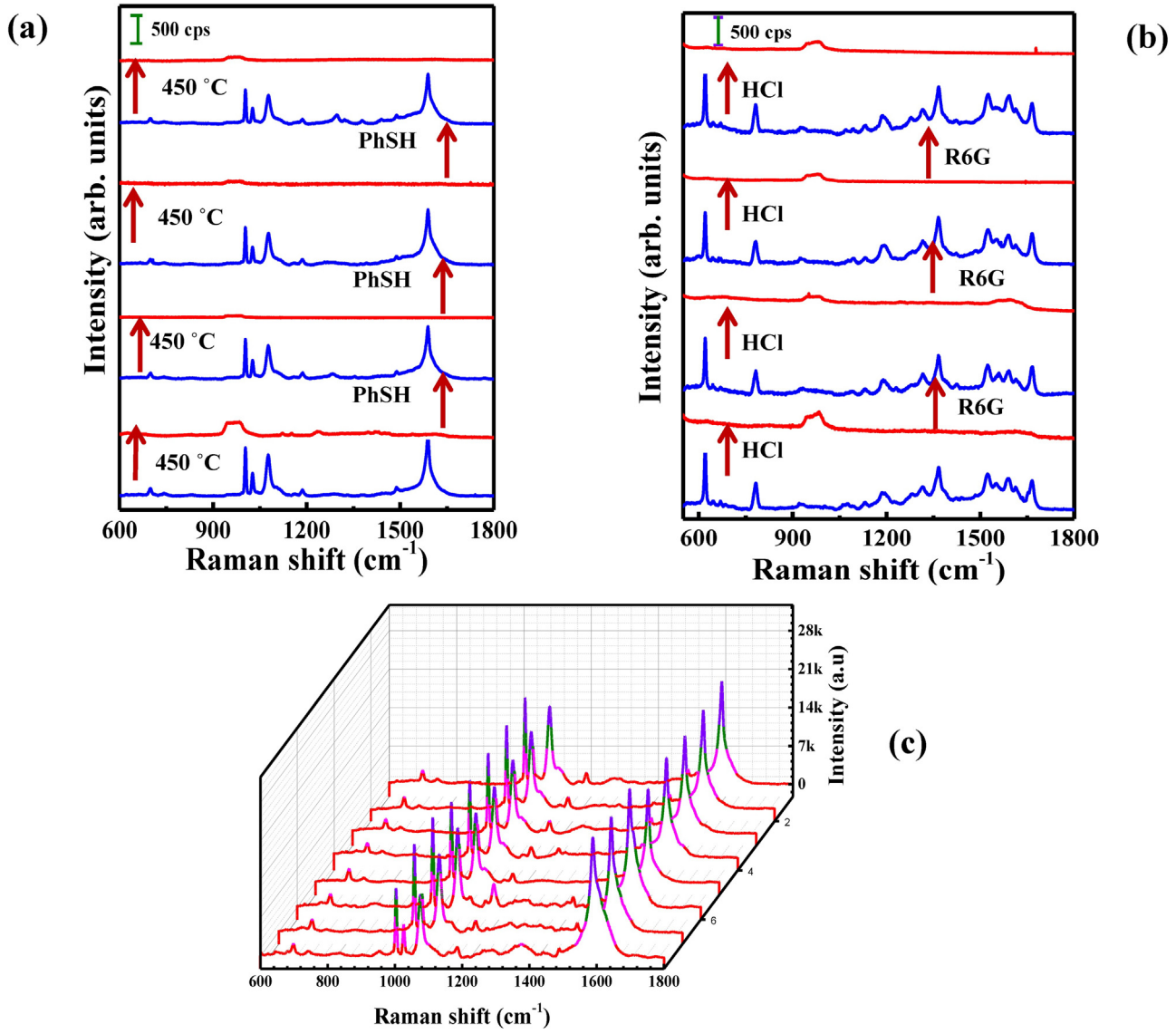

Fig. 4. (a) Reusability of the SiNPLs-SERS sensor through heat treatment for four cycles, red and blue represent SERS spectra after dropcasting and heating up to 450 °C in air, respectively. (b) Reusability of the SiNPLs-SERS sensor through chemical treatment for four cycles, red and blue indicates SERS spectra after dropcasting and HCl wash for 10 min, respectively. (c) The SERS spectra of thiophenol taken from eight random positions of the SiNPLs-SERS sensor. (For interpretation of the references to color in this figure legend, the reader is referred to the web version of this article.)

nanoparticles grafted to amyloid beta through extra cysteine, have been used for obtaining SERS of amyloid beta [35]. No such functionalization of substrate or capture probe for protein is required in our case. Nucleic acids (deoxyribonucleic acid, DNA), are another important class of biomolecules due to their role in multiplex detection and were also studied as depicted in Fig. 3(e). The typical protein concentration used for SERS of HSA, BSA, Lysozyme, DNA and a Beta was 10^{-6} M with acquisition time of 90 s. The detailed SERS peak assignments for all the proteins are provided in Supplementary information.

Two different types of cells; red blood cells (RBC) and bacterial cells (*E. coli*) were investigated for their surface proteins. RBCs were taken from human blood and then washed in PBS. A 10 μL drop (25,000 RBC per μL) was cast over the sample and was left to dry in air for an hour. The Raman spectra of RBC were recorded in 532 nm laser with an accumulation time of 90 s. The SERS spectra of RBC are assigned to lipids, carbohydrates and proteins present on its cell membrane. These surface proteins can be used as biomarkers for disease detection as they are altered by pathogens, diseases and medication. SiNPLs-SERS sensor could be used in malaria detection as it can differentiate between healthy and infected RBCs based upon surface biomarkers and receptors [39]. Fig. 3(f) represents SERS spectrum of healthy RBC (# represents 2nd order Si peak) with dominant peaks at 1130, 1170, 1305, 1375, 1589 and 1645 cm^{-1}. There is an overall increase in intensity in the SERS spectrum of schizont stage of malaria infected RBC(i-RBC) along with the additional peaks at 730, 970, 1080 and 1431 cm^{-1} as shown in Fig. 3(g). The peaks marked by "*" show changes in the relative intensities and/or are new peaks of schizont stage of malaria. SERS of *E. coli*, a Gram negative bacterium, was also done to show the utility of SiNPLs-SERS sensor in bacterial detection, presented in Fig. 3(h). SiNPLs-SERS sensor was also used for detecting fluorescent dye molecules like Fluorescein isothiocyanate (FITC) and $DiSC_3(5)$ (3,3′-Dipropylthiadicarbocyanine Iodide), as shown in Fig. 3(i) and (j), respectively. These fluorogenic probe dyes are used in bio-imaging of membranes. Schematic diagram for the interaction of cells and differently charged proteins with the SiNPLs-SERS sensor is shown in Fig. 3(k).

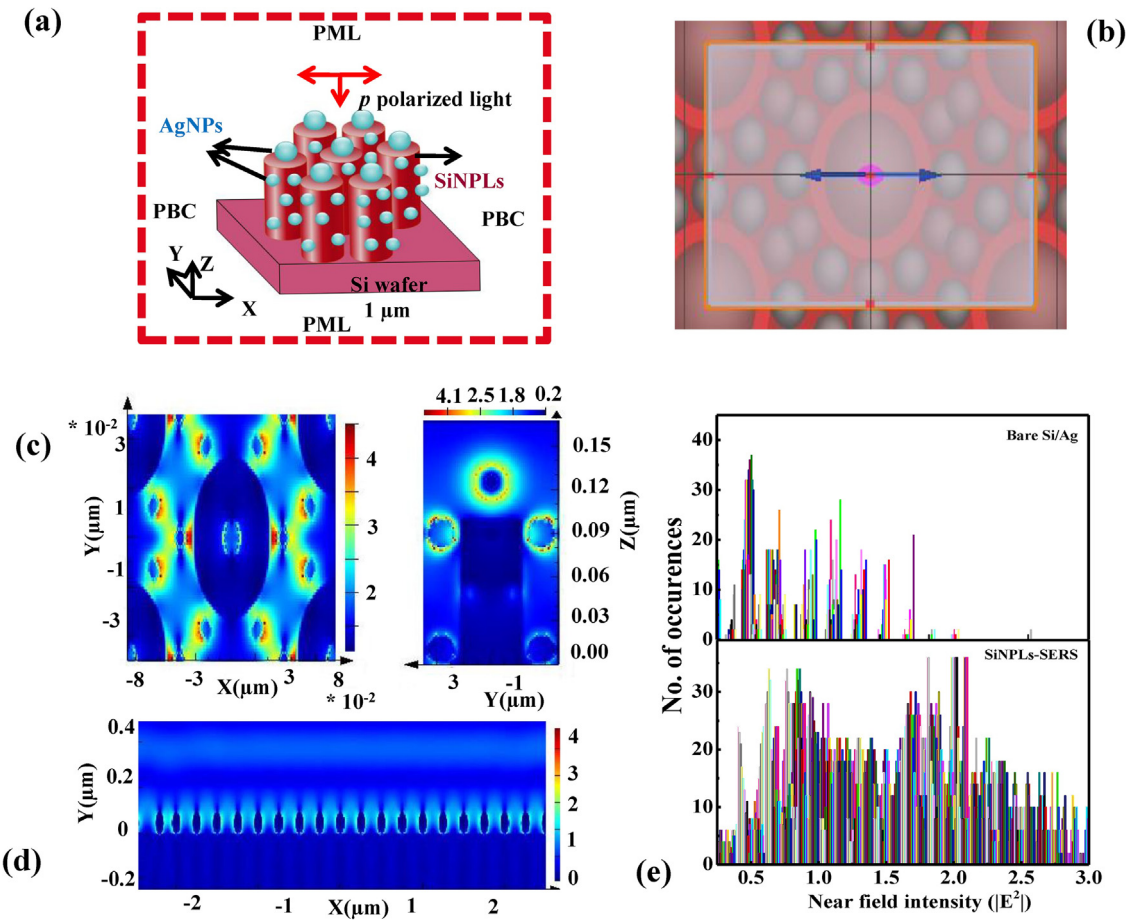

Fig. 5. (a) The schematic representation of the FDTD simulation. (b) Top view of the simulation region (c) and (d) Plasmonic hotspot distribution for the SiNPLs-SERS and bare Si sensor, respectively. (e) Histogram shows the near field intensity distribution for bare and SiNPLs-SERS sensor.

In order to check the reusability of the SiNPLs-SERS sensor, we have recorded the SERS spectra of PhSH at 450 °C as shown in Fig. 4(a). The observable SERS peaks of PhSH have not been observed at 450 °C. This indicates the complete evaporation of PhSH without affecting the SiNPLs-SERS sensor. Moreover, the SERS intensity remains almost unaffected after cyclic heating. The reusability of the substrate has been also investigated under chemical treatment using R6G as an analyte. The substrates were immersed in HCl after recording the spectra of 1 μM R6G. The SERS spectra of R6G before and after HCl immersion are shown in Fig. 4(b). A slight intensity variation is observed in the cyclic chemical treatment. This is ascribed to the leaching and displacement of AgNPs during the chemical immersion. The cyclic SERS measurements ensure the stability and reusability of the SiNPLs-SERS sensor under chemical and heat treatments. In order to check the shelf time of the AgNPs, we have performed the SERS experiments after 6 months of sample preparation. It could be seen that the sample still shows the SERS signal even after 6 months, but the intensity was less. We have recorded the SERS spectra after treating with HCl and the SERS spectrum showed an improved intensity for thiophenol and the results are presented in Supplementary Fig. S3(c). These results indicate that the SiNPLs-SERS substrate is reusable even after 6 months with simple HCl treatment.

The reproducibility of the substrates was verified by recording spectra of PhSH with concentration 1 mM from eight randomly selected regions of SiNPLs-SERS sensor as shown in Fig. 4(c). The intensity and unique characteristics of PhSH is well maintained in all the spectra. The relative standard deviation (RSD) is used to reassert the reproducibility of the SiNPLs-SERS sensor. The RSD values for the peaks at 1003, 1027, 1077 and 1576 cm^{-1} are 0.086, 0.076, 0.054, 0.068, respectively. It could be seen that the RSD values of all the characteristic peaks stay less than 0.08. The negligibly small RSD values indicate the homogeneity and the excellent reproducibly of the SiNPLs-SERS substrates. The reproducibility spectra of the other sets of samples (SiNPLs of roughness 355 nm and 1 μm) were also checked and the corresponding results are shown in Supplementary Fig. S4(a) and (b).

The decoration of AgNPs on the SiNPLs leads to a very interesting plasmonic behavior due to the coupling and guiding of light through the AgNPs as well as the SiNPLs. To get a deeper insight to the plasmonic behavior of the SiNPLs-SERS sensor, we have performed 3D FDTD. The schematic model for the FDTD simulation and the top view of the simulation region are shown in Fig. 5(a) and (b), respectively. Based on the observations from FESEM, the SiNPLs of size 80 nm, height 1 μm, periodicity 100 nm and AgNPs of average size 50 nm are modeled in the simulation. Fig. 5(c) represents the FDTD near field intensity plots (represents hot spot distributions) for the SiNPLs-SERS sensor. The plasmonic hot-spot distribution of bare Si sensor (bare Si coated with AgNPs) is also shown in Fig. 5(d) for comparison. The near field intensity $|E|^2$ was calculated based on the number of occurrences in the simulation area for the SiNPLs-SERS sensor and bare Si sensor, as shown in Fig. 5(e). The number of occurrences for SiNPLs-SERS sensor is much higher than the bare Si sensor, which accounts for the very high enhancement of SiNPLs-SERS sensor. The simulation results shows that the additional surface area provided by the SiNPLs leads to increase in the number density of AgNPs as compared to bare Si sensor, leading to tremendous increase in hot spots and thus EF.

4. Conclusion

In summary, a simple and reliable method is presented for developing highly efficient SERS biosensors based on periodic array of SiNPLs decorated with AgNPs. High quality, well ordered arrays of SiNPLs were fabricated by PS nanosphere lithography and metal assisted chemical etching. The uniformity in the arrangement of SiNPLs has led to a homogeneous distribution of AgNPs, which resulted in high enhancement factor and excellent reproducibility. The SiNPL-SERS sensor exhibited a maximum enhancement factor of 2.4×10^8 and sensitivity up to 10^{-13} M for R6G. Moreover, the intensity showed an exponential relationship with the concentration of R6G from 10^{-7} to 10^{-13} M. The positively and negatively charged proteins such as BSA, HSA and lyzozyme could be differentiated through the SERS spectra recorded using uncharged AgNPs on the SiNPLs. The hydrophobic amyloid beta proteins responsible for alzheimers disease were detected using SiNPLs-SERS sensor. The detection of *E. coli* bacterial cells, healthy and malaria infected RBC using SiNPLs-SERS makes our substrate more versatile than the other SERS substrates. Finally, the tremendous increase in the hotspot distribution of our substrate was described and compared with the bare Si sensor using FDTD simulation.

Acknowledgments

The authors are thankful to the Director, CSIR-NAL for his support and encouragement. BRNS (Project No.: U-1-125) is thanked for SRF fellowship to K. P. SA's fellowship was supported by JNCASR-DST. CN would like to thank Sheikh Saqr Laboratories for funding.

Appendix A. Supplementary data

Supplementary data associated with this article can be found, in the online version, at http://dx.doi.org/10.1016/j.snb.2017.07.088.

References

[1] S. Schlucker, Surface-enhanced Raman spectroscopy: concepts and chemical applications, Angew. Chem. Int. Ed. 53 (2014) 4756–4795.
[2] L.M. Chen, Y.N. Liu, Surface-enhanced Raman detection of melamine on silver-nanoparticle-decorated silver/carbon nanospheres: effect of metal ions, ACS Appl. Mater. Interfaces 3 (2011) 3091–3096.
[3] S.M. Nie, S.R. Emery, Probing single molecules and single nanoparticles by surface enhanced Raman scattering, Science 275 (1997) 1102–1106.
[4] B. Sharma, R.R. Frontiera, A.I. Henry, E. Ringe, R.P.V. Duyne, SERS: materials, applications, and the future, Mater. Today 15 (2012) 16–25.
[5] S. Kumar, P. Goel, J.P. Singh, Flexible and robust SERS active substrates for conformal rapid detection of pesticide residues from fruits, Sens. Actuators B: Chem. 241 (2017) 58–577.
[6] J.F. Bryche, B. Bélier, B. Bartenlian, G. Barbillon, Low-cost SERS substrates composed of hybrid nanoskittles for a highly sensitive sensing of chemical molecules, Sens. Actuators B: Chem. 239 (2017) 795–799.
[7] J.F. Li, Y.F. Huang, Y. Ding, Z.L. Yang, S.B. Li, X.S. Zhou, F.R. Fan, W. Zhang, Z.Y. Zhou, D.Y. Wu, B.Z. Ren, L. Wang, Z.Q. Tian, Shell-isolated nanoparticle-enhanced Raman spectroscopy, Nature 464 (2010) 392–395.
[8] C. Eliasson, A. Loren, J. Engelbrektsson, M. Josefson, J. Abrahamsson, K. Abrahamsson, Surface-enhanced Raman scattering imaging of single living lymphocytes with multivariate evaluation, Spectrochim. Acta 61 (2005) 755–760.
[9] S.P. Ravindranath, Y. Wang, J. Irudayaraj, SERS driven cross-platform based multiplex pathogen detection, Sens. Actuators B: Chem. 152 (2011) 183–190.
[10] T.V. Dinh, SERS chemical sensors and biosensors: new tools for environmental and biological analysis, Sens. Actuators B: Chem. 29 (1995) 183–189.
[11] E. Hutter, J.H. Fendler, Exploitation of localized surface plasmon resonance, Adv. Mater. 16 (2004) 1685–1706.
[12] S. Nie, S.R. Emory, Probing single molecules and single nanoparticles by surface-enhanced Raman scattering, Science 275 (1997) 1102–1106.
[13] H. Liang, Z. Li, W. Wang, Y. Wu, H. Xu, Highly surface roughened flower-like silver nanoparticles for extremely sensitive substrates of surface-enhanced Raman scattering, Adv. Mater. 21 (2009) 4614–4618.
[14] P. Strobbia, E. Languirand, M.B. Cullum, Recent advances in plasmonic nanostructures for sensing: a review, Opt. Eng. 54 (2015) 100902–100909.
[15] Z. Zhan, R. Xu, Y. Mi, H. Zhao, Y. Lei, Highly controllable surface plasmon resonance property by heights of ordered nanoparticle arrays fabricated via a nonlithographic route, ACS Nano 9 (2015) 4583–4590.
[16] Q. Fu, Z. Zhan, J. Dou, X. Zheng, R. Xu, M. Wu, Y. Lei, Highly reproducible and sensitive SERS substrates with Ag inter-nanoparticle gaps of 5-nm fabricated by UTAM technique, ACS Appl. Mater. Interfaces 7 (2015) 13322–13328.
[17] G. Santoro, S. Yu, M. Schwartzkopf, P. Zhang, S.K. Vayalil, J.F.H. Risch, M.A. Rubhausen, M. Hernández, C. Domingo, S.V. Roth, Silver substrates for surface enhanced Raman scattering: correlation between nanostructure and Raman scattering enhancement, Appl. Phys. Lett. 104 (2014) (243107-5).
[18] V. Liberman, C. Yilmaz, T.M.S. Bloomstein, Somu, Y. Echegoyen, A. Busnaina, S.G. Cann, K.E. Krohn, M.F. Marchant, M.A. Rothschild, Nanoparticle convective directed assembly process for the fabrication of periodic surface enhanced Raman spectroscopy substrates, Adv. Mater. 22 (2010) 4298–4302.
[19] C. Fernandez-Lopez, C. Mateo-Mateo, R.A. Alvarez-Puebla, J. Perez-Juste, I. Pastoriza-Santos, L.M. Liz-Marzan, Highly controlled silica coating of PEG-capped metal nanoparticles and preparation of SERS-encoded particles, Langmuir 25 (2009) 13894–13899.
[20] K. Kneipp, Y. Wang, H. Kneipp, L.T. Perelman, I. Itzkan, R.R. Dasari, S.F. Michael, Single molecule detection using surface-enhanced Raman scattering (SERS), Phys. Rev. Lett. 78 (1997) 1667–1670.
[21] J.F. Betz, W.W. Yu, Y. Cheng, I.M. White, Simple SERS substrates: powerful, portable and full of potential, Phys. Chem. Chem. Phys. 16 (2014) 2224–2225.
[22] M. Jin, G. He, H. Zhang, J. Zeng, Z. Xie, Y. Xia, Shape-controlled synthesis of copper nanocrystals in an aqueous solution with glucose as a reducing agent and hexadecylamine as a capping agent, Angew. Chem. Int. Ed. 50 (2011) 10560–10564.
[23] L. Polavarapu, K.K. Manga, K. Yu, P.K. Ang, H.D. Cao, J. Balapanuru, K.P. Loh, Q.H. Xu, Alkylamine capped metal nanoparticle inks for printable SERS substrates, electronics and broadband photodetectors, Nanoscale 3 (2011) 2268–2274.
[24] X.M. Lin, Y. Cui, Y.H. Xu, B. Ren, Z.Q. Tian, Surface-enhanced Raman spectroscopy: substrate-related issues, Anal. Bioanal. Chem. 394 (2009) 1729–1745.
[25] Q. Yu, S. Braswell, B. Christin, J. Xu, P.M. Wallace, H. Gong, D. Kaminsky, Surface-enhanced Raman scattering on gold quasi-3D nanostructure and 2D nanohole arrays, Nanotechnology 21 (2010) 355301–355308.
[26] C.M. Hsu, S.T. Connor, M.X. Tang, Y. Cui, Wafer-scale silicon nanopillars and nanocones by Langmuir-Blodgett assembly and etching, Appl. Phys. Lett. 93 (2008) 133109–133113.
[27] U.S. Dinish, F.C. Yaw, A. Agarwal, M. Olivo, Development of highly reproducible nanogap SERS substrates: comparative performance analysis and its application for glucose sensing, Biosens. Bioelectron. 26 (2011) 1987–1992.
[28] N. Gupta, D. Gupta, S. Aggarwal, S. Siddhanta, C. Narayana, H.C. Barshilia, Thermally stable plasmonic nanocermets grown on microengineered surfaces as versatile surface enhanced Raman spectroscopy sensors for multianalyte detection, ACS Appl. Mater Interfaces 6 (2014) 22733–22742.
[29] K.A. Willets, V. Duyne, Localized surface plasmon resonance spectroscopy and sensing, Annu. Rev. Phys. Chem. 58 (2007) 267–297.
[30] Y.F. Li, J.H. Zhang, S.J. Zhu, H.P. Dong, Z.H. Wang, Z.Q. Sun, J.R. Guo, B. Yang, Low-cost fabrication of large area sub-wavelength anti-reflective structures on polymer film using a soft PUA mold, J. Mater. Chem. 19 (2009) 1806–1810.
[31] Y.L. Deng, Y.J. Juang, Black silicon SERS substrate: effect of surface morphology on SERS detection and application of single algal cell analysis, Biosens. Bioelectron. 53 (2014) 201437–201442.
[32] J.D. Caldwell, O. Glembocki, F.J. Bezares, N.D. Bassim, R.W. Rendell, M. Feygelson, M. Ukaegbu, R. Kasica, L. Shirey, C. Hosten, Plasmonic nanopillar arrays for large- area, high-enhancement surface- enhanced Raman scattering sensors, ACS Nano 5 (2011) 4046–4055.
[33] M.R. Gartia, Z. Xu, E. Behymer, H. Nguyen, J.A. Britten, C. Larson, R. Miles, M. Bora, A.S.-P. Chang, T.C. Bond, G.L. Liu, Rigorous surface enhanced Raman spectral characterization of large-area high-uniformity silver-coated taperedsilica nanopillar arrays, Nanotechnology 21 (2010) 395701–395709.
[34] M.S. Schmidt, J. Hubner, A. Boisen, Large area fabrication of leaning silicon nanopillars for surface enhanced Raman spectroscopy, Adv. Mater. 24 (2012) 11–18.
[35] L. Guerrini, R. Arenal, B. Mannini, F. Chiti, R. Pini, P. Matteini, R.A. Alvarez-Puebla, SERS detection of amyloid oligomers on metallorganic-decorated plasmonic beads, ACS Appl. Mater Interfaces 7 (2015) 9420–9428.
[36] H. Zhou, D. Yang, N.P. Ivleva, N.E. Mircescu, R. Niessner, C. Haisch, SERS detection of bacteria in water by in situ coating with Ag nanoparticles, Anal. Chem. 86 (2014) 1525–1533.
[37] J. Chen, X. Wu, Y.W. Huang, Y. Zhao, Detection of *E. coli* using SERS active filters with silver nanorod array, Sens. Actuators B: Chem. 191 (2014) 485–490.
[38] S. Siddhanta, V. Thakur, N. Chandrabhas, S.M. Shivaprasad, Universal metal-semiconductor hybrid nanostructured SERS substrate for biosensing, ACS Appl. Mater. Interfaces 4 (2012) 5807–5812.
[39] F. Chen, B.R. Flaherty, C.E. Cohen, D.S. Peterson, Y. Zhao, Direct detection of malaria infected red blood cells by surface enhanced Raman spectroscopy, Nanomedicine 12 (2016) 1445–1451.
[40] P. Karadan, S. John, A.A. Anappara, N. Chandrabhas, H.C. Barshilia, Evolution mechanism of mesoporous silicon nanopillars grown by metal-assisted chemical etching and nanosphere lithography: correlation of Raman spectra and red photoluminescence, Appl. Phys. A 22 (2016) 669–674.

[41] P. Karadan, A.A. Anappara, V.H.S. Moorthy, N. Chandrabhas, H.C. Barshilia, Improved broadband and omnidirectional light absorption in silicon nanopillars achieved through gradient mesoporosity induced leaky waveguide modulation, RSC Adv. 6 (2016) 109157–109170.

Biographies

Prajith Karadan is studying for a Ph.D. degree at National Institute of Technology, Calicut and working as senior research fellow at CSIR-National Aerospace Laboratories, Bangalore. His research interests are fabrication of Si nanostructures for antireflection, surface enhanced Raman spectroscopy and photodetector applications.

Shantanu Aggarwal is studying for a Ph.D. degree at Jawaharlal Nehru Centre for Advanced Scientific Research, Bangalore. His research interests are fabrication of novel substrates for surface enhanced Raman spectroscopy studies of proteins, cells and dyes.

Aji A. Anappara is an Assistant Professor in the Department of Physics, National Institute of Technology Calicut. His areas of expertise are optics of carbon quantum dots, photochemical fuels based on nanomaterial hybrids, Optoelectronics of graphene and graphene/nanometal hybrids.

Chandrabhas Narayana is a Professor of Chemistry and Physics of Materials Unit, Jawaharlal Nehru Centre for Advanced Scientific Research, Bangalore. He has more than two decades of experience in the area of surface enhanced Raman spectroscopy, Brillouin scattering, High pressure Raman spectroscopy, etc.

Harish C. Barshilia is working as a Chief Scientist at CSIR-National Aerospace Laboratories, Bangalore. He works in the area of high temperature solar selective coatings, PVD coatings and multifunctional nanostructured coatings for antireflection, self cleaning, etc.